Study of the agreement between binary neutron star ejecta models derived from numerical relativity simulations

Henkel, A.; Foucart, F.; Raaijmakers, G.; Nissanke, S.

DOI
10.1103/PHYSREVD.107.063028

Publication date
2023

Document Version
Final published version

Published in
Physical Review D - Particles, Fields, Gravitation and Cosmology

Study of the agreement between binary neutron star ejecta models derived from numerical relativity simulations

Amelia Henkel,[1] Francois Foucart,[1] Geert Raaijmakers,[2] and Samaya Nissanke[2]
[1]*Department of Physics, University of New Hampshire, 9 Library Way, Durham, New Hampshire 03824, USA*
[2]*GRAPPA Institute of High-Energy Physics, University of Amsterdam, Science Park 904, 1098 XH Amsterdam, Netherlands*

(Received 25 July 2022; accepted 14 February 2023; published 24 March 2023)

Neutron star mergers have recently become a tool to study extreme gravity, nucleosynthesis, and the chemical composition of the Universe. To date, there has been one joint gravitational and electromagnetic observation of a binary neutron star merger, GW170817, as well as a solely gravitational observation, GW190425. In order to accurately identify and interpret electromagnetic signals of neutron star mergers, better models of the matter outflows generated by these mergers are required. We compare a series of ejecta models to see where they provide strong constraints on the amount of ejected mass expected from a system, and where systematic uncertainties in current models prevent us from reliably extracting information from observed events. We also examine 2396 neutron star equations of state compatible with GW170817 to see whether a given ejecta mass could be reasonably produced with a neutron star of said equation of state, and whether different ejecta models provide consistent predictions. We find that the difference between models is often comparable to or larger than the error generally assumed for these models, implying better constraints on the models are needed. We also note that the extrapolation of outflow models outside of their calibration window, while commonly needed to analyze gravitational wave events, is extremely unreliable and occasionally leads to completely unphysical results.

DOI: 10.1103/PhysRevD.107.063028

I. INTRODUCTION

The observation of gravitational waves from a binary neutron star merger (GW170817) and of an associated short gamma-ray burst (GRB 170817A) and kilonova signal (AT2017gfo) ushered the world into the era of multimessenger astronomy [1]. Binary neutron star (BNS) mergers are of great scientific interest for the wealth of information encoded in the observable signals that they power. They can provide insights into strong gravity [2], nucleosynthesis and the origin of heavy elements [3–5], the dynamics and formation mechanisms of gamma ray bursts (GRBs) [6], and the neutron star equation of state (EOS) [7,8].

Their gravitational wave signal provides important information about the source parameters, such as the mass and spin of each neutron star (e.g., [8]). The UV/optical/IR signal powered by the radioactive decay of elements produced during r-process nucleosynthesis (*kilonova*) is mostly dependent on the mass, velocity, morphology, and composition of the outflows [9,10]. As these quantities are themselves function of the properties of the merging neutron stars, kilonovae provide us with another way to study the properties of merging binaries, complementing gravitational wave observations. Additionally, any well-localized electromagnetic (EM) counterpart to a BNS merger will help break degeneracies in the parameters estimated from gravitational wave measurements.

The ejecta from BNS mergers is often described using a two-component model (e.g., [5,11,12]): the dynamical ejecta, ejected during the merger itself or the first few milliseconds postcontact, and the disk wind ejecta, produced up to a few seconds after the merger. The dynamical ejecta is typically faster, and may include a neutron-rich component associated with the tidal disruption of a neutron star and a less neutron-rich component due to shocks and oscillations in the forming neutron star remnant (see, e.g., [13,14]). The wind ejecta is typically slower, though both its velocity and composition may be significantly impacted by physical processes that are not fully included in many existing postmerger simulations (magnetohydrodynamics, neutrino transport). Physically, it may originate from a range of physical processes including magnetically driven outflows [15,16], neutrino-driven outflows [17,18], and viscous outflows [19]. Disk outflows produced by these various processes likely have different velocities, temperatures, and compositions.

Given the limited number of neutron star merger simulations performed so far, candidate electromagnetic signals to BNS mergers are typically analyzed using an approximate analytical model fitted to the result of

numerical simulations. To date, a number of models have been developed to constrain the dynamics and outflows of BNS mergers (e.g., [10,20–24]). These models typically provide predictions for the properties of the dynamical ejecta or of the postmerger remnant disk, without further distinguishing between, e.g., different types of dynamical ejecta. For the scope of this paper, and to allow for meaningful model comparisons, we thus work within this approximate two-component ejecta model as well.

These analytical models which have been fitted to the results of numerical relativity (NR) simulations have some known limitations. For example, recent work by Nedora *et al.* [24] clearly demonstrated that the predictions of these fits can be heavily influenced by the level of microphysics included in the simulations used to calibrate them. In this manuscript, we attempt to answer a slightly different question, namely how robust inferences made about the properties of neutron stars are to the choice of fitting formula. This remains an important open question because some models do not include reliable error bars for their predictions, while models that do include errors bars only cover a limited region of parameter space and may lead to significantly larger systematic errors when used outside of their intended region of validity—something that should ideally be avoided, yet is common practice when analyzing existing electromagnetic signals from neutron star mergers, due to the lack of models covering the entire parameter space of interest.

We structure our paper in the following way: first, we introduce the ejecta models considered in this study. We then present a comparison of these models, and show where they currently agree and disagree, under the simplifying assumption that both neutron stars have the same radius. We later drop the constant radius assumption and apply the ejecta models to a series of EOSs consistent with gravitational wave observation GW170817 to see if current observations can elucidate the true dense matter EOS. Finally, we conclude with a discussion of our results, drawing attention to the cases similar to the BNS events GW170817 and GW190425.

II. EJECTA MODELS

A. Dynamical ejecta models

First, we visit three fitting formulas for the amount of dynamical ejecta emitted from neutron star mergers, taken from Kruger and Foucart [23] (hereafter KF), Dietrich and Ujevic [21] (hereafter DU), and Nedora *et al.* [24] (hereafter NAL). The mass predicted from these models is shown in Fig. 1. A summary of these formulae, as well as the disk ejecta formulae discussed further in Section IIB, can be found in Table I. We note that these formulas do not distinguish between the cold, neutron-rich tidal ejecta and the hot, less neutron-rich ejecta produced by the collision of the neutron star cores, and do not tell us anything about the geometry of the ejecta. We do not investigate here the impact of these issues on kilonovae light curves, but it is worth noting that even if these formulas were exact, they would not be sufficient to predict the kilonova signals associated with the dynamical ejecta. NAL introduced some fitting formulas providing partial information about the composition and geometry of the outflows, but they point out that the accuracy of these formulas is significantly limited by the small number of numerical relativity simulations with sufficiently advanced microphysics that reported the observables fitted in their work.

DU present a phenomenological fit of the mass, energy, and velocities of dynamical ejecta derived from a large series of numerical relativity simulations ($N = 172$). They use simulations presented in Hotokezaka *et al.* [25], Bauswein *et al.* [26], Dietrich *et al.* [27], Lehner *et al.* [28], Sekiguchi *et al.* [29], and Dietrich *et al.* [30]. Their dataset combines results from general relativistic grid structured codes with results employing a smoothed particle hydrodynamics code under the conformal flatness approximation. It includes piecewise polytropic and tabulated EOSs, as well as simulations with and without neutrino treatment. As this study only considers dynamical ejecta, and no wind ejecta, Dietrich and Ujevic note that their estimates can provide a lower bound for the luminosity of EM observables.

Their fit for the dynamical ejecta mass is as follows:

$$\frac{M_{\rm ej}^{\rm fit}}{10^{-3}} = \left[a\left(\frac{M_2}{M_1}\right)^{1/3}\left(\frac{1-2C_1}{C_1}\right) + b\left(\frac{M_2}{M_1}\right)^{\rm n} + c\left(1-\frac{M_1}{M_1^*}\right)\right]M_1^* + 1 \leftrightarrow 2 + d, \tag{1}$$

where $a = -1.35695$, $b = 6.11252$, $c = -49.43355$, $d = 16.1144 M_\odot$, and $n = -2.5484$; M^* is the baryonic mass, M is the gravitational mass in isolation, $C = GM/Rc^2$ is the compactness, and R is the radius of the neutron star. In this manuscript, we adopt the convention $M_1 \leq M_2$, though Eq. (1) is symmetric in the masses of the two objects. Additionally, as we do not always have enough information about the EOS of dense matter to self-consistently calculate M^*, we approximate M^* using the quasiuniversal relation between mass and compactness [31]

$$M^* = M\frac{(1+0.6C)}{(1-0.5C)}. \tag{2}$$

KF developed formulas for the dynamical ejecta of BNS and black hole-neutron star (BHNS) systems, as well as the disk mass for BNSs. Their dynamical ejecta fit for BHNS systems is outside the scope of this work, as we only consider BNSs; their disk mass ejecta fit is described in greater detail in Sec. II B. KF's fit is similar to DU's, but does not depend on baryonic mass. In their fitting formulas, they aim for analytical simplicity as well as physically reasonable extrapolation toward high-compactness stars.

TABLE I. Information about the dynamical ejecta (dyn. ej.) and disk mass (disk) models considered in this work. From left to right, the columns indicate (i) the name of the model; (ii) type of outflow; (iii) information about the simulations to which the models are calibrated; (iv) the models' input parameters; (v) the range of mass ratios to which the models are calibrated; and (vi) the uncertainty associated with each model, when quoted.

Source	Model	Simulations	Inputs	Calibrated Q	Uncertainty
DU [21]	Dyn. Ej.	172 sims from [25–30]	M_1, M_2, C_1, C_2	0.48–1.0	$0.004M_\odot$
KF [23]	Dyn. Ej.	200 sims from [21,32]	M_1, M_2, C_1, C_2	0.48–1.0	$0.004M_\odot$
NAL [24]	Dyn. Ej.	324 sims from [22,24,29,33–37]	$\tilde{\Lambda}$, $\tilde{Q}$	0.54–1.0	$0.5M_{ej} + 5 \times 10^{-5} M_\odot$
KF [23]	Disk	57 sims from [22,32]	$M_{\rm low}$, $C_{\rm low}$	0.775–1.0	$0.5M_{\rm disk} + 5 \times 10^{-4} M_\odot$
DAL [38]	Disk	73 sims from [22,30,32,39]	Q, $M_{\rm tot}$, $M_{\rm th}$	0.571–1.0	Not quoted
RAL [22]	Disk	59 sims performed by RAL	$\tilde{\Lambda}$	0.85–1.0	$0.5M_{\rm disk} + 5 \times 10^{-4} M_\odot$
NAL [24]	Disk	119 sims from [22,24,29,33–37]	$\tilde{\Lambda}$, $\tilde{Q}$	0.54–1.0	$0.5M_{\rm disk} + (5 \times 10^{-4}) M_\odot$

They also derive their fits from a slightly larger region of parameter space; namely, they base their work off of NR simulations from Radice *et al.* [22] and Kiuchi *et al.* [32], in addition to those used by DU. These additional simulations include, among other things, more asymmetric binaries than in the original dataset.

Their dynamical ejecta fit for BNSs is given as

$$\frac{M_{\rm dyn}}{10^{-3}} = \left(\frac{a}{C_1} + b \frac{M_2^{\rm n}}{M_1^{\rm n}} + c C_1 \right) M_1 + (1 \leftrightarrow 2); \quad (3)$$

here, $a = -9.3335$, $b = 114.17$, $c = -337.56$, and $n = 1.5465$. They too define M_1 as the less massive star.

NAL presents fitting formulas for the dynamical ejecta of BNS mergers based on a polynomial in mass ratio $\tilde{Q}$ and reduced tidal deformability $\tilde{\Lambda}$, defined as

$$\tilde{\Lambda} = \frac{16}{13} \frac{(M_2 + 12M_1) M_2^4 \Lambda_2}{M^5} + (2 \leftrightarrow 1). \quad (4)$$

In this convention, $\tilde{Q} = M_2/M_1 \geq 1$ and $M = M_2 + M_1$. Additionally, Λ_i is the dimensionless tidal deformability of either neutron star, and is defined as $\Lambda_i = (2/3) k_i^{(2)} C_i^{-5}$. Within this, $k_i^{(2)}$ is the tidal Love number and C_i the compactness; see Damour and Nagar [40] for a more detailed discussion of $k_i^{(2)}$. We note that as for the baryonic mass, in the absence of a well-defined EOS we will often find ourselves in this manuscript without a unique way to calculate $k_i^{(2)}$, and thus Λ_i. When that is the case, we rely once more on known quasiuniversal relations, specifically the compactness-Love number relation of [41]:

$$C = 0.371 - 0.0391 \ln \Lambda + 0.00105 (\ln \Lambda)^2. \quad (5)$$

NAL obtain their fitting formula from a suite of recent NR simulations (available at Nedora *et al.* [24]) with varying levels of realism in their treatment of the composition of the star and neutrino transport. While they present fitting formulas with two distinct polynomial orders and including or excluding simulations with better/worse microphysics, that they then apply to a multitude of binary parameters, we only consider here their "recommended" fitting formula applied to the dynamical ejecta mass and disk mass. The fitting formula is as follows:

$$P_2^2(\tilde{Q}, \tilde{\Lambda}) = b_0 + b_1 \tilde{Q} + b_2 \tilde{\Lambda} + b_3 q^2 + b_4 \tilde{Q} \tilde{\Lambda} + b_5 \tilde{\Lambda}^2. \quad (6)$$

For the dynamical ejecta, they provide best-fit parameters $b_0 = -1.32$, $b_1 = -0.382$, $b_2 = -4.47 \times 10^{-3}$, $b_3 = -0.339$, $b_4 = 3.21 \times 10^{-3}$, and $b_5 = 4.31 \times 10^{-7}$.

B. Disk mass models

Fitting formulas for the mass remaining in an accretion disk around the remnant black hole (or neutron star) after a BNS merger have also been provided in multiple works. These formulas are typically fit to a lower number of simulations than dynamical ejecta formulas, as not all numerical relativity simulations report remnant disk masses. Additionally, the definition of the disk mass itself varies between different studies, complicating comparisons between different sets of simulations. Most notably, reported disk masses are sensitive to the time at which they are measured, and to the definition of the boundary between the "disk" and "neutron star" in neutron star-disk systems. They are however crucial to kilonovae modeling, as most BNS mergers likely eject more mass through disk winds than dynamical ejecta: from Fig. 2, we see that disks are often much more massive than the dynamical ejecta, and 20–50% of that disk might end up unbound in disk winds [15,19]. The disk ejecta models used in this study are summarized in Table I and are elaborated upon further here.

KF provides a fitting formula for the disk mass in BNS merger remnants, based on the subset of simulations used for the dynamical ejecta model that provides disk mass information. The disk mass fit for BNSs they arrive at is as follows:

$$M_{\rm disk} = M_1 \max\{5 \times 10^{-4}, (a C_1 + c)^d\}, \quad (7)$$

where M_1 and C_1 are the gravitational mass and compactness of the less massive neutron star, respectively, and the

best-fit coefficients are $a = -8.1324$, $c = 1.4820$, and $d = 1.7784$. Their fit has an associated uncertainty of

$$\Delta M_{\rm disk} = 0.5 M_{\rm disk} + 5 \times 10^{-4} M_\odot. \tag{8}$$

We also consider the disk mass fitting formula provided by Dietrich *et al.* [38], hereafter DAL. Their fit is derived from a series of 73 numerical relativity simulations performed by Kiuchi *et al.* [32], Radice *et al.* [22], Dietrich *et al.* [30], and Hotokezaka *et al.* [39]. Their model takes a similar form to their previous results in Coughlin *et al.* [42], but improves upon it by including mass-ratio dependent fitting parameters. They arrive at the following disk mass fit:

$$\log_{10}(M_{\rm disk}) = \max\left(-3, a\left(1 + \beta \tanh\left(\frac{c - M/M_{\rm thresh}}{d}\right)\right)\right), \tag{9}$$

where the threshold mass $M_{\rm thresh}$ is the value of the initial gravitational mass $M_1 + M_2$ of the BNS above which we expect prompt collapse to a black hole. Here, a and b are given as

$$a = a_0 + \delta a \xi,$$
$$b = b_0 + \delta b \xi,$$

and ξ can be expressed as

$$\xi = \frac{1}{2} \tanh\left(\beta(Q - Q_{\rm trans})\right). \tag{10}$$

The best-fit coefficients are $a_0 = -1.581$, $\delta a = -2.439$, $b_0 = -0.538$, $\delta b = -0.406$, $c = 0.953$, $d = 0.0417$, $\beta = 3.910$, and $Q_{\rm trans} = 0.900$. In practice, $M_{\rm thresh}$ is dependent on the maximum mass of nonrotating neutron stars, and of the radius of those neutron stars. To estimate the value of $M_{\rm thresh}$, DAL use the method presented in Agathos *et al.* [43]. When we work under the constant radius assumption, we do not have any information about the maximum mass of neutron stars. To circumvent this, we developed an approximate relationship between the maximum compactness $C_{\rm max}$ and $R_{1.4}$, the radius of a $1.4 M_\odot$ star, as the compactness is an easily calculable quantity. When comparing the quantities for each EOS used later in our study (see Sec. III C), we observed a slightly positive linear relationship between them. A larger radius of the $1.4 M_\odot$ star corresponds to a larger value of $M_{\rm thresh}$. We then calculate the threshold mass according to

$$M_{\rm thresh}(R_{1.4}) = (0.22 R_{1.4} + 0.4) M_\odot. \tag{11}$$

We note that the relation is not as reliable as existing quasiuniversal relations, and is only used to get a reasonable estimate of $M_{\rm thresh}$ when using an unphysical EOS. When we work with EOSs that do not simply assume a constant radius in Sec. III C, we are able to obtain $M_{\rm thresh}$ using the method of Agathos *et al.* [43].

Additionally, we consider the model provided by NAL. Their polynomial fit for the dynamical ejecta [Eq. (6)] is also used for the disk mass. For the disk mass, they have that $b_0 = -1.85$, $b_1 = 2.59$, $b_2 = 7.07 \times 10^{-4}$, $b_3 = -0.733$, $b_4 = -8.08 \times 10^{-4}$, and $b_5 = 2.75 \times 10^{-7}$.

Lastly, we employ the results from Radice *et al.* [22], hereafter RAL. They study the mass ejection, nucleosynthetic yields, and electromagnetic counterparts of BNS mergers based on 59 high-resolution numerical relativity simulations. They employ four finite temperature, composition dependent EOSs (SFHo, BHB$\Lambda\phi$, DD2, and LS220) to constrain current estimates on merger outflows and ejecta properties. Their models are calibrated to a mass ratio range of 0.85–1.0. Their data are fit by the following expression:

$$\frac{M_{\rm disk}}{M_\odot} = \max\left\{10^{-3}, \alpha + \beta \tanh\left(\frac{\tilde{\Lambda} - \gamma}{\delta}\right)\right\}, \tag{12}$$

where $\alpha = 0.084$, $\beta = 0.127$, $\gamma = 567.1$, and $\delta = 405.14$. They also quote the uncertainty in the disk mass as

$$\Delta M_{\rm disk} = 0.5 M_{\rm disk} + 5 \times 10^{-4} M_\odot. \tag{13}$$

III. METHODS

A. Comparing dynamical ejecta models

First, we compare dynamical ejecta models from DU, KF, and NAL. We do this to see for what radii and mass ratios the models agree, and to measure their level of agreement over the parameter space. For each figure, we fix the chirp mass. We then generate a range of 100 mass ratios $Q = M_1/M_2$ evenly spaced between 0.5 and 1.0 (where $M_1 < M_2$), which allows us to calculate the individual masses M_1 and M_2 with the following relation:

$$M_2 = M_c \frac{(Q+1)^{1/5}}{Q^{3/5}}. \tag{14}$$

In practice, M_c will typically be fairly well measured from gravitational wave observations, but Q will come with significant uncertainties. Additionally, measurements of Q are partially degenerate with measurements of the spins of the neutron stars. In this manuscript, we focus on uncertainties due solely to the choice of the ejecta model, and thus assume fixed values of M_c and Q; yet in actual observations the uncertainty in Q would certainly have to be taken into account.

We then generate 100 values of the neutron star radius from 10 to 14 km, working under the assumption that both neutron stars have the same radius: $R_1 = R_2$. The use of a constant radius is clearly an approximation. As evidenced by Fig. 3, however, a broad range of masses corresponds to

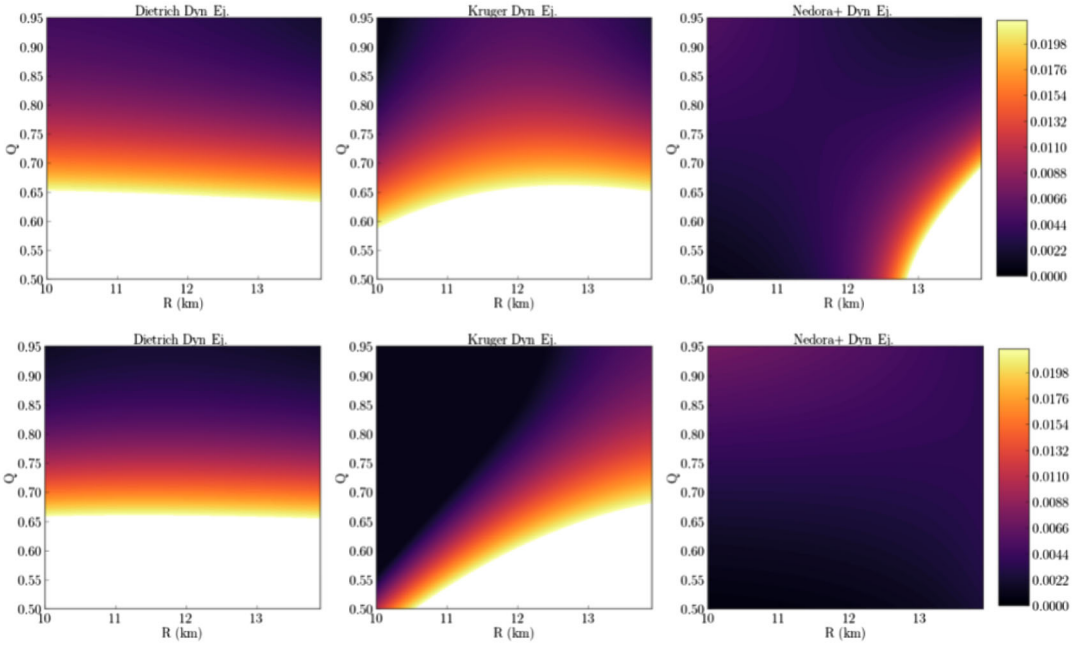

FIG. 1. Dynamical ejecta mass predicted by Dietrich and Ujevic's model (left); Kruger and Foucart's model (center); and Nedora *et al.*'s model (right). The colormaps are in units of solar masses; the chirp mass is $M_c = 1.186M_\odot$ for the top panel and $M_c = 1.44M_\odot$ for the lower panel. We truncate values above $0.022M_\odot$, to make the more reliable regions of the parameter space easier to study. At high-mass ratio, the extrapolation of fitting formulas outside of their range of applicability leads to extremely large predicted masses that have never been observed so far in simulations ($\gtrsim 0.06M_\odot$).

a very small range of radii for most EOSs consistent with existing nuclear physics and astrophysical constraints—and visualizing models in the 2D space of mass ratios and radii is easier than in the infinite dimensional space of mass ratio and EOSs. We will lift this simplifying assumption later when considering predictions for specific EOSs.

We select chirp masses $M_c = 1.44M_\odot$, the value associated with GW190425 [44], and $M_c = 1.186M_\odot$, the value associated with GW170817 [1]. After calculating the component masses, the dynamical ejecta mass for each combination of R and Q is calculated according to Eqs. (1), (3), and (6). We then plot the dynamical ejecta from each model as color gradients on a radius vs mass ratio grid, as seen in Fig. 1. We note that while a mass ratio $Q \sim 0.5$ is highly unlikely for the low chirp mass case (the lower mass star would have $M \sim M_\odot$, which is not necessarily impossible but incredibly rare; see Doroshenko *et al.* [45]), it is more plausible for the high chirp mass case ($M_1 \sim 1.2M_\odot$, $M_2 \sim 2.4M_\odot$). While BNSs with $Q \sim 0.5$ are unlikely given the small range of possible neutron star masses, we deliberately probe a large parameter space to ascertain the models' behavior at extreme–and less well-studied—regions of the parameter space.

It is evident from Fig. 1 that for both the DU and KF dynamical ejecta models, a higher ejecta mass is predicted for more unequal mass mergers. This is to be expected, as unequal mass mergers are associated with more tidal deformation. We can also observe a stronger dependence on radius in KF's model relative to DU or NAL. For a fixed mass ratio, KF predicts different amounts of ejecta depending on the radius; when $Q = 0.7$ and $M_c = 1.44M_\odot$, for example, the model predicts negligible ejecta when the NS radii are $\sim$10 km, but almost $0.02M_\odot$ of ejecta for NSs with $R \sim 14$ km. One objective of their model was to account for the expected lack of ejecta from highly compact stars near the equal mass limit, a phenomena that is physically understood but not automatically reflected by fitting formulas due to the lack of numerical simulations in that regime. This is particularly visible in the higher chirp mass case, where a larger fraction of the systems are expected to undergo prompt collapse to a black hole. Because the component masses are a function of M_c, a larger chirp mass will correspond to more massive NSs; see Eq. (14). All else being equal, the figures generated using a larger M_c will demonstrate more cases of prompt collapse (no observed ejecta). The NAL model shows very different qualitative behavior, especially outside of the regions where most numerical relativity simulations used to calibrate these models are found (near equal mass, noncollapsing systems). We believe part of this discrepancy can be attributed to the fact that NAL's quadratic ejecta model takes a different functional form than KF and DU. Additionally, it is a function of $\tilde{Q}$ and $\tilde{\Lambda}$, whereas the other two models are functions of the component masses and compactness. It is important to note that while the KF model does recover what we expect to be the correct limit for small radii—namely, that when NSs become extremely compact ($R \to 0$), no ejecta is produced—there is no evidence that it performs better than

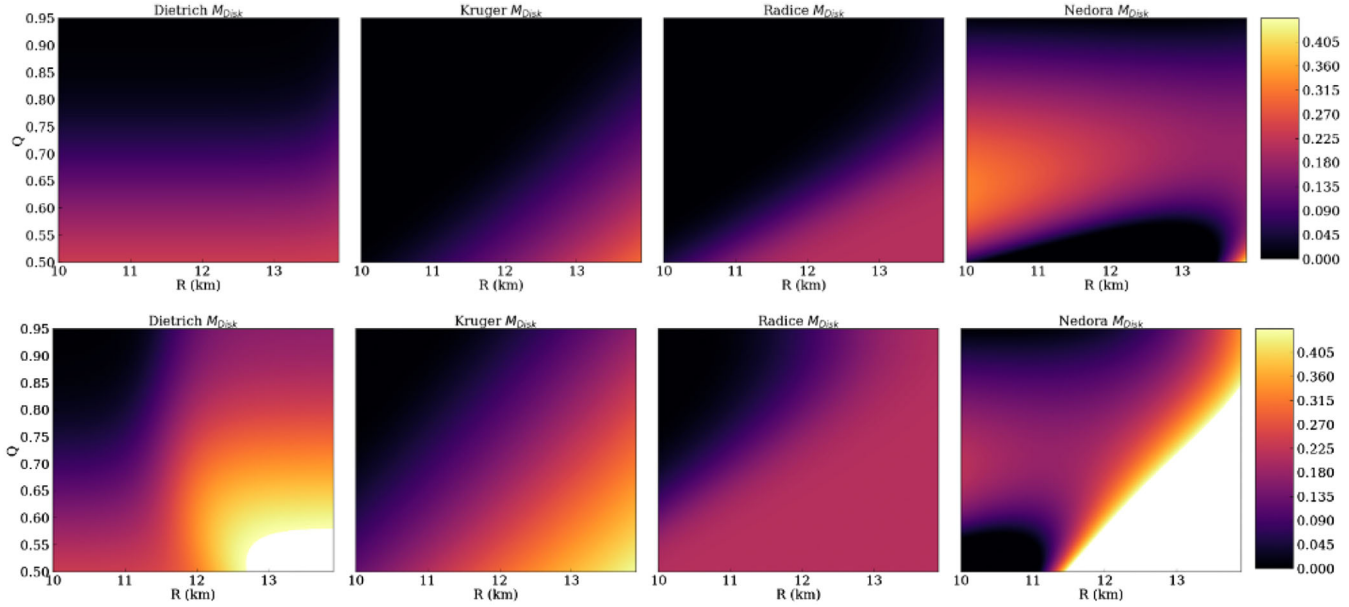

FIG. 2. Disk mass calculated with each of the four disk mass models considered in this study. The figures in the top panel have a chirp mass of $M_c = 1.186M_\odot$; the figures in the bottom panel have $M_c = 1.44M_\odot$. We truncate the ejecta values for $M_{\rm disk} > 0.449M_\odot$ because the values quickly become unphysical outside of their domains.

the other models at more moderate radii. For example, Nedora *et al.* [24] showed that the NAL and KF models have, despite their very visible qualitative differences, comparable fitting residuals when fitted to their chosen datasets, while Camilletti *et al.* [46] showed that existing dynamical ejecta models compare poorly to numerical simulations for a GW190425-like system. There is also no particular reason to believe that one model is more accurate when extrapolating to very asymmetric systems; in fact, all models predict unrealistically large ejecta mass for asymmetric systems, and it is more likely than not that they are all very inaccurate in that regime (the models predict masses well above $0.06M_\odot$, while no simulation used to calibrate the model has seen ejected masses above $0.06M_\odot$, and most simulations find dynamical ejecta masses $M_{\rm ej} \lesssim 0.01M_\odot$). Using these models for asymmetric binaries can thus be particularly dangerous if no corrections are applied, especially when assessing the impact of mergers on r-process nucleosynthesis (see, e.g., [47]).

B. Disk mass model comparison

Next, we perform the same model comparison procedure with the aforementioned disk mass models: KF (from [23]), DAL (from [38]), RAL (from [22]), and NAL (from [24]). This is done to determine if any constraints about a BNS EM observation can be made given some level of agreement between said models.

Referring to Fig. 2, we can immediately observe that some predicted disk masses become unphysical for increasingly unequal mass cases, similar to the dynamical ejecta. For example, the NAL model predicts a disk containing upwards of $16M_\odot$ for low compactness (larger R, smaller Q) when $M_c = 1.188M_\odot$. For ease of visualization of the results, we truncate any values in excess of $0.5M_\odot$ in our figures.

All the disk mass models considered in this work predict relatively low disk masses ($M_{\rm disk} \lesssim 0.01M_\odot$) for nearly equal mass systems; this is to be expected, as the most efficient way to form massive accretion disks in BNS mergers is through the tidal disruption of a lower mass star by its more massive companion. That less compact (larger R) stars produce more massive disks is well-captured in the DAL, KF, and RAL models. NAL has a more complex behavior as a function of R, especially for high-mass systems, due to the chosen functional form for the model (nearly all models from NAL are quadratic with a saddle point close to or within the fitting region).

As for the dynamical ejecta models, the disk mass models show particularly significant disagreement for GW190425-like systems. Camilletti *et al.* [46] showed that for GW190425-like systems, the KF model is accurate (within its relatively large error bars) in the parts of the high-mass parameter space covered by their simulations (for $Q \gtrsim 0.65$), though we caution again about inferring too much from that result about the quality of the model in other regions of the BNS parameter space.

C. Equation of state

The previous sections assumed a constant-radius EOS; an assumption convenient for visualizing the results but that does not exactly match realistic EOSs. For a more consistent treatment of the nuclear EOS, we consider a suite

of 2396 neutron star EOSs. The EOSs employed in this study are a series of best-fit "spectral" EOSs consistent with GW170817 data. More information about the EOSs included in this study can be found in Abbott *et al.* [8], while the theoretical framework on which these EOSs are based can be found in Lindblom [48]. Each EOS in the publicly available master file contains best-fit values for the spectral EOS parameters $\gamma_0, \gamma_1, \gamma_2$, and γ_3, as well as the pressure at a reference density. Information about the mass, radius, and tidal deformability for each EOS can then be obtained from these data (see Raaijmakers *et al.* [49]).

The main practical use of the analytical models discussed here is to attempt to determine whether the binary parameters of a given system—or a series of binary parameters from multiple events—can be used to reliably rule out certain EOSs, and thus constrain the true neutron star EOS. In this manuscript, we test how robust these inferences are to the choice of model assuming extremely simplified constraints from potential observations.

First, we define a fiducial system's total ejecta mass $M_{\rm tot}$ (dynamical ejecta and disk outflows), chirp mass, and mass ratio. In practice, the chirp mass and mass ratio are only known up to the potentially large uncertainties in gravitational wave parameter estimation, while the derivation of the total ejecta mass from, e.g., a kilonova signal is a nontrivial process that depends on the morphology, composition, and velocity of the ejecta as well as nuclear physics and radiation transport uncertainties. In order to directly study uncertainties due to the current modeling of the total ejecta, however, we ignore these important complications for now, and do not consider any uncertainty in the fiducial ejecta mass, chirp mass, or mass ratio. We define the fiducial ejecta mass as the total amount of dynamical ejecta and unbound disk ejecta; in practice, this quantity would have to be inferred from kilonova observations (see, e.g., Raaijmakers *et al.* [49] and Coughlin *et al.* [42]). Defining M_c and Q sets the component masses of our system M_1 and M_2. In the figures discussed in this section, M_c and Q are fixed in each panel, and thus each panel corresponds to some constant M_1 and M_2.

Second, we obtain the radii R_1 and R_2 and tidal deformabilities Λ_1 and Λ_2 corresponding to M_1 and M_2 respectively, for each EOS. From these values, we can calculate the compactness C of each neutron star as well as the reduced tidal deformability $\tilde{\Lambda}$ of the binary. These quantities all serve as inputs for the ejecta models considered in this work.

Then we calculate the dynamical ejecta as a function of the aforementioned inputs for each EOS. Each panel considers *either* the model presented by KF, DU, *or* NAL; the dynamical ejecta model considered for each column is indicated in its title.

Next, we calculate the disk ejecta, also functions of the aforementioned quantities, for each EOS, assuming that a fraction $f_{\rm disk}$ of the accretion disk is ejected as disk wind in the seconds following the merger. Given uncertainties $\sigma_{\rm dyn}$ and $\sigma_{\rm disk}$ in $M_{\rm dyn}$ and $M_{\rm disk}$ and assuming $f_{\rm disk} \in [f_{\rm low}, f_{\rm high}]$, we calculate a "window" of possible values for the total ejected mass:

$$M_{\rm min} = (M_{\rm dyn} - \sigma_{\rm dyn}) + f_{\rm low}(M_{\rm disk} - \sigma_{\rm disk}),$$
$$M_{\rm max} = (M_{\rm dyn} + \sigma_{\rm dyn}) + f_{\rm high}(M_{\rm disk} + \sigma_{\rm disk}).$$

Doing so provides a range of ejecta values that, according to the model, is compatible with the input parameters M_c, Q, and the chosen EOS. The fiducial ejecta mass is then compared to each calculated ejecta mass window to see if the fiducial mass falls within the calculated range. For the KF and DU figures, we present a comparison of KF's, DAL's, and RAL's disk mass models. For the NAL figures, we overlay the performance results of KF's, DAL's, RAL's, and NAL's disk ejecta models. This is done to more clearly draw a comparison between what ejecta models of different functional forms predict. NAL's models have the largest variation compared with others, and are the most sensitive to extrapolation (because the function is a polynomial fit to the data), so this is also done to show how well the other models agree with each other without NAL included. We hold fixed the fractional range of unbound disk mass, with $f_{\rm low} = 0.1$ and $f_{\rm high} = 0.4$. We initially considered two windows, 10–40% and 20–25%, to check whether better constraints on the fraction of unbound disk mass impact our results, but found that doing so does not provide any additional information at this point—the differences between models and fit uncertainties have a stronger impact on our results.

If for a given EOS the fiducial ejecta mass falls within the window of acceptable masses for all models under consideration, then that EOS is assumed to be compatible with the fiducial observation. If it falls outside of that window for all models, the EOS is incompatible with that observation. Finally, if the fiducial ejecta mass falls within the allowed region for some models but not others, no robust inference can be made about that EOS—and inferences made without considering modeling uncertainties may be inaccurate. For each panel, we overlay the mass-radius curve of each of the 2396 EOSs, color coded according to whether the fiducial binary parameters agree with none (black), some (red), or all (green) of the disk mass models. We demonstrate this process in Fig. 3.

Our results are presented in Figs. 4 and 5. We consider the same chirp masses as before, $1.186M_\odot$ and $1.44M_\odot$, and the two mass ratios $Q = 0.9$ and $Q = 0.72$. We use $Q = 0.72$ to demonstrate highly unequal mass mergers; any mass ratio more extreme produces values of M_1 and M_2 which fall outside the range allowed by some of the EOSs. We ignore mass ratios $Q \lesssim 0.7$ as we have already seen that the existing models are unreliable in that regime. Finally, we initialize fiducial ejecta masses of $0.05M_\odot$, which is similar to GW170817, and $0.005M_\odot$, to study which

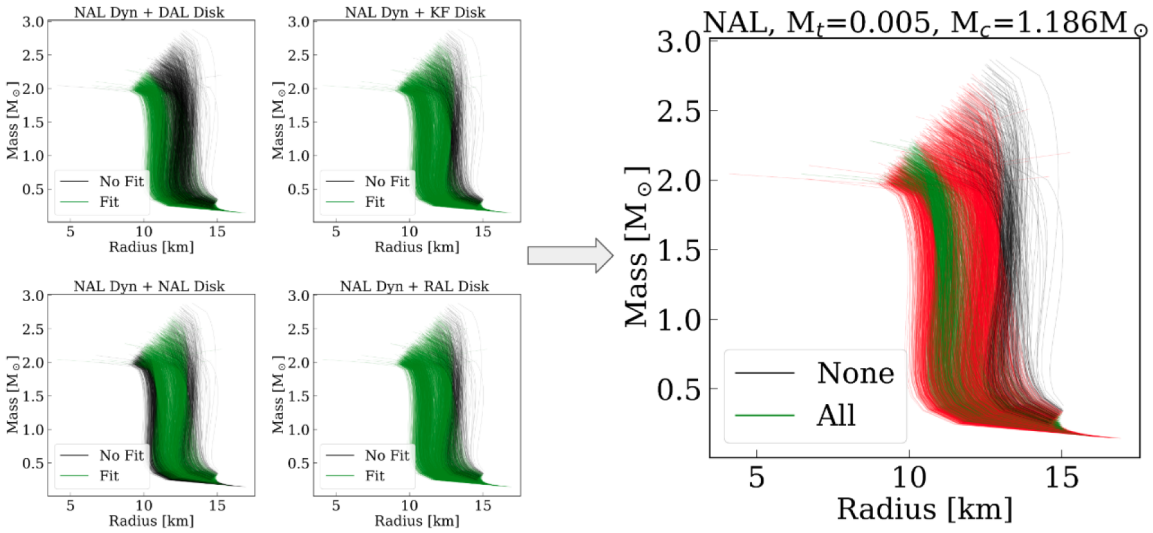

FIG. 3. A demonstration for how the subsequent figures in this paper are produced. For the suite of EOSs considered in this work, we determine whether each one can reproduce ejecta in agreement with a preselected fiducial value, and color code their mass-radius relations accordingly. This is done by, for a given set of input parameters (M_c and Q), calculating the dynamical ejecta according to one model, and then calculating the disk ejecta according to multiple models for comparison, and then overlaying where the results agree and disagree. The larger figure shows an overlay of the results from (NAL dyn. ej.) + (disk ej.) for the four models considered in this work. The four smaller panels show the results for each of the disk models.

systems are compatible with effectively negligible mass ejection (such as, possibly, GW190425).

We present all possible configurations of the input parameters in Figs. 4 and 5, with each row corresponding to the same M_c, M_t, and Q for ease of comparison. Looking first at Fig. 4, we can see that for $M_c = 1.186M_\odot$, all models agree that EOSs with typical radii $R \gtrsim 12$ km (for $\sim 1.4M_\odot$ neutron stars) are capable of ejecting $\sim 0.05M_\odot$. The KF and DU models also agree that typical radii $R \lesssim (11\text{–}12)$ km are consistent with an ejected mass of $0.005M_\odot$. The NAL model does not however agree with that last statement, predicting significant mass ejection for neutron stars with $R \lesssim 11$ km (specifically when combining both their dynamical ejecta and disk mass models, as shown in Fig. 3). Consistently ruling out an EOS (i.e., having an EOS appear black for all models) seems to be more difficult. For $M_t = 0.005M_\odot$, we reject approximately 35, 25, and 7% of the least compact EOSs when using the dynamical ejecta models of KF, DU, and NAL. For $M_t = 0.05M_\odot$, the NAL model does not allow us to consistently rule out any EOS (the other two panels rule out $\sim 30\%$ of the EOSs for those parameters).

The results for $M_c = 1.44M_\odot$ and $Q = 0.9$ can more easily be analyzed if we first look at the bottom panels of Fig. 2. There, we see that the DAL, KF, and RAL disk models predict the production of very low mass disks at that mass ratio, while NAL's disk model predicts a slightly more massive disk. As a result, when combining the first three disk models with the KF and DU dynamical ejecta models, we accept nearly all EOSs for $M_t = 0.005M_\odot$ and nearly none for $M_t = 0.05M_\odot$ (i.e., those models predict that the latter observation would be extremely unlikely). The NAL disk mass model, on the other hand, predicts that for $M_c = 1.44M_\odot$ and $Q = 0.9$ we may get $M_t = 0.05M_\odot$, but not $M_t = 0.005M_\odot$. Hence, nearly all EOSs are red on the right panel of the third and fourth rows of Fig. 4. Using the NAL model for both the dynamical ejecta mass and the disk mass makes most EOSs consistent with $M_t = 0.05M_\odot$; using the NAL dynamical ejecta model in combination with another disk mass model is consistent with $M_t = 0.005M_\odot$. This is clearly a case where inferences made about the properties of a system from combined GW and EM observations may be significantly impacted by the choice of outflow model made in the analysis.

We now turn the focus of our discussion to Fig. 5, which corresponds to $Q = 0.72$. Looking first to the top row which corresponds to $M_c = 1.186M_\odot$ and a fiducial mass $M_t = 0.005M_\odot$, we can see that the KF and DU panels agree that such an unequal mass system cannot produce negligible ejecta. The narrative shifts for the NAL panel, where NAL's low dynamical ejecta appear to be the source of disagreement. We can see from Fig. 1 that while DU and KF predict significant dynamical ejecta for nearly all radii in this regime, NAL predicts almost none. The second row of Fig. 5, which corresponds also to $M_c = 1.186M_\odot$ but now a fiducial mass $M_t = 0.05M_\odot$, demonstrates consistent results between the different dynamical ejecta models, but disagreements at the level of the disk models. This case does not robustly rule out any EOS, but it does consistently identify viable ones—here, EOSs with typical radii $\gtrsim 12$ km.

The fourth row of Fig. 5, with $M_c = 1.44M_\odot$ and $M_t = 0.05M_\odot$, shows significant disagreement between disk

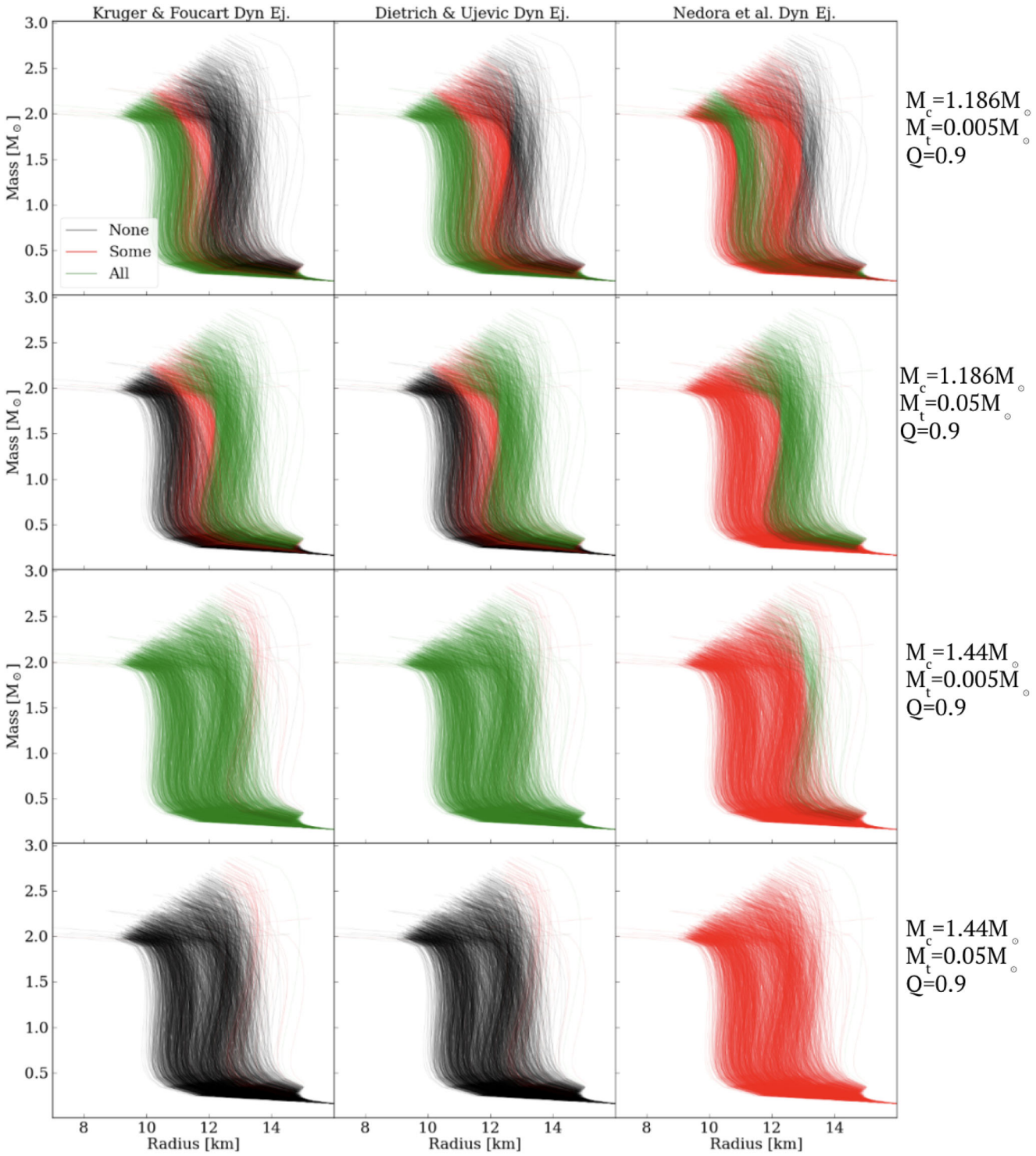

FIG. 4. Mass-radius relationships for 2396 EOSs from [8]. The figures above employ one of three dynamical ejecta models, KF, DU, or NAL; one of two fiducial ejecta masses, $0.05M_\odot$ and $0.005M_\odot$; and one of two chirp masses, $1.186M_\odot$ (in agreement with observations of GW170817) and $1.44M_\odot$ (in agreement with GW190425). The KF and DU dyn. ej. figures overlay a comparison of KF, DAL, and RAL disk ejecta, whereas the NAL dyn. ej. figures overlay a comparison of KF, DAL, RAL, and NAL disk ejecta. All figures here correspond to systems with a fixed mass ratio $Q = 0.9$.

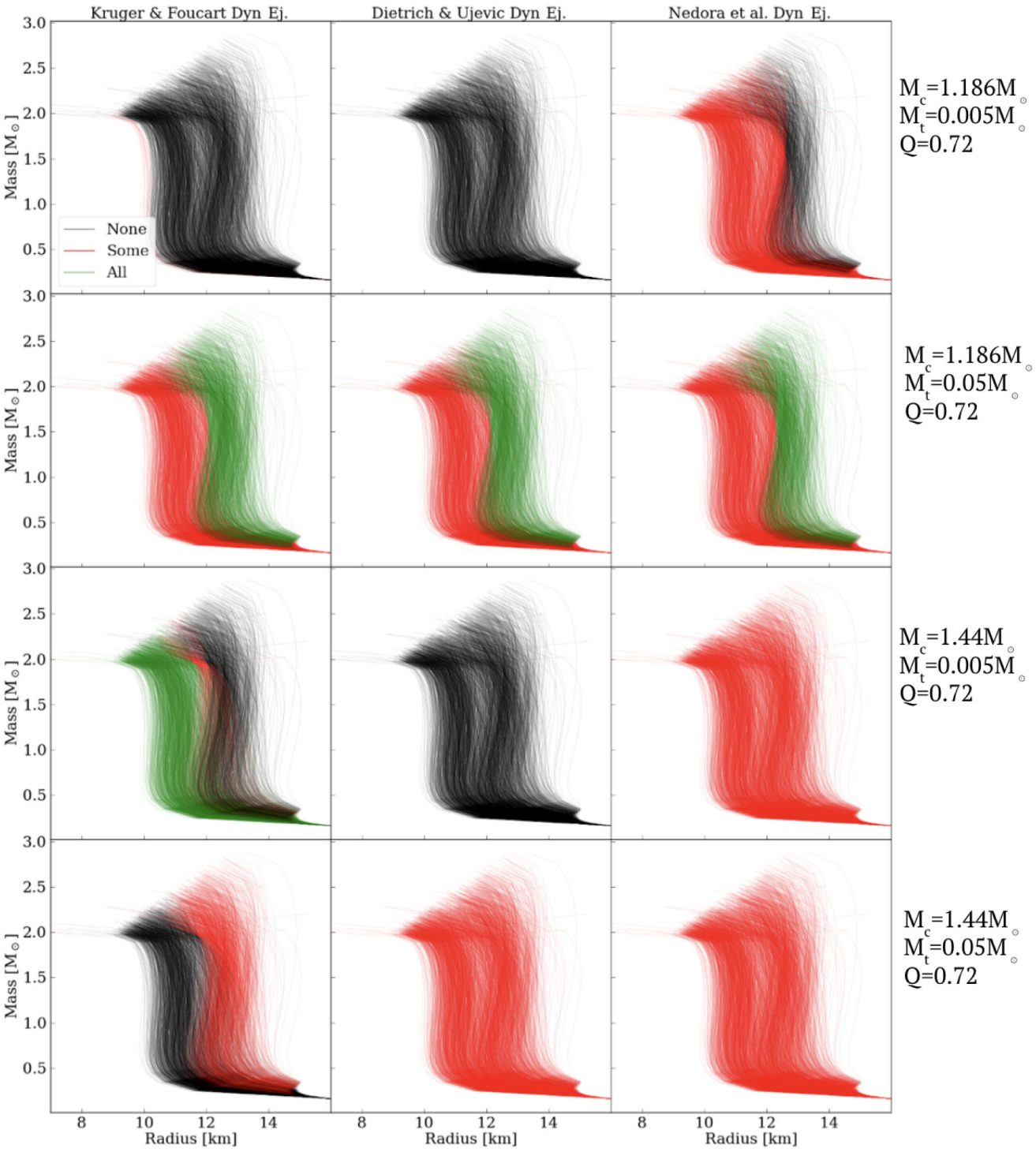

FIG. 5. The same scenarios as Fig. 4, but with mass ratio $Q = 0.72$.

mass models and between dynamical ejecta models. While the KF dynamical ejecta model disallows the most compact EOSs for all disk mass models, the different disk model disagrees for neutron stars with radii $R \gtrsim 12$ km. For the DU and NAL dynamical ejecta models, the disk mass models provide different predictions for all EOSs. The models are consistently unable to make robust predictions in this region of parameter space. Similarly, we would be unable to draw robust conclusions from an observed system with $M_c = 1.44M_\odot$ and $M_t = 0.005M_\odot$. When using DU's dynamical ejecta model, all EOSs are disallowed; when using KF's dynamical ejecta model, only the more compact EOSs with radii $R \lesssim 12$ km are allowed; and when using NAL's dynamical ejecta model, the different

disk mass models provide different predictions for the entire parameter space. While the results here disagree with each other, we can see that they are consistent with what is predicted in Fig. 1. DU's dynamical ejecta model produces upward of $0.01M_\odot$ at $Q = 0.72$ for all radii, disqualifying all EOSs when $M_t = 0.005M_\odot$. We can also see from Fig. 2 that NAL predicts, for most radii, a larger disk mass than the other three disk models.

IV. DISCUSSION

We have considered a series of dynamical ejecta and disk mass models for BNSs and estimated their predictive power by measuring agreement between models for a given system. We find that regions where all existing models are consistent are quite rare, and that we should thus be cautious about making inferences about the parameters of BNS systems using just one of these models—even when accounting for the models' stated uncertainties. We recommend to at least compare results with different ejecta models in order to get a sense of modeling uncertainties for a given system.

In more detail, we find that for the dynamical ejecta models, DU and KF demonstrate a stronger dependence on mass ratio than is seen for NAL. That more unequal mass systems produce relatively more ejecta compared with equal mass systems is well captured in DU's and KF's models, but not by NAL. We note that this is likely explained by NAL's model being a function of different parameters compared with DU and KF (Q and $\tilde{\Lambda}$ vs $M_{1,2}$ and $C_{1,2}$), and that the model takes a different functional form compared with the two other models. Of the three models, KF demonstrates the strongest dependence on radius, which is an intentional feature meant to capture the different behavior of BNS systems of varying compactness. All of the models begin to diverge to unrealistically high values as we probe increasingly unequal mass systems, which is due to the models being used outside of the parameter space to which they were calibrated. For this reason, it can often be problematic to extrapolate ejecta fits. We also wish to highlight that the differences between what the models predict is often of the order of the actual predicted ejecta mass.

We perform the same study on the disk mass models considered in this work. The models consistently predict low/no disk masses for compact (small R), equal-mass systems, which agrees with our current understanding that such mergers result in prompt collapse to a black hole. However, different models have different thresholds for when ejecta is or is not produced. All disk models with the exception of NAL produce significant ejecta for increasingly unequal mass systems; for $Q \sim 0.55$–0.6, NAL predicts negligible disk mass. As was the case for the dynamical ejecta, we see that the differences between the models are comparable in magnitude to the models' predictions.

Relative to NAL, we observe stronger dependence on radius for the disk mass models from KF, DAL, and RAL, which is particularly evident for the smaller chirp mass panel of Fig. 2. For the high chirp mass panel of Fig. 2, disagreement between models is most pronounced at low radii. The lower chirp mass panel demonstrates divergence between models in several parts of the parameter space, but most notably for high radii. As was the case for the dynamical ejecta, the differences between disk mass models are at times comparable in magnitude to the models' predictions.

We then studied a series of 2396 EOSs from a parameter estimation performed for GW170817, and determined whether each EOS could reproduce some injected fiducial ejecta mass given the dynamical ejecta and disk mass models we have considered. We find that there is slightly stronger agreement between models for the $Q = 0.9$ case, with some fiducial observations consistently ruling out/accepting a subset of the proposed EOSs. However, for most fiducial observations (and particularly for more asymmetric systems), the large variations in the predictions of different fitting formulas should urge us to proceed with extreme caution when attempting to derive information about the EOS of neutron stars from kilonovae signals powered by BNS mergers—at least when that process relies on current models for the mass of the outflows.

For the case most similar to GW170817 ($M_c = 1.186M_\odot$, $Q = 0.9$, $M_{\rm tot} = 0.05M_\odot$), we see all models agree that the least compact (largest radius and, typically, largest maximum mass) EOSs are consistent with such a system. This is one of the only parts of the parameter space where all models produce consistent results. Most models predict that the more compact EOSs should be ruled out by such an observation (and NAL, which does not at $Q = 0.9$, would rule out compact NSs as well if we had chosen a slightly more symmetric mass ratio).

Notably, we are unable to draw any conclusions about the NS EOS from the case most similar to GW190425 ($M_c = 1.44M_\odot$, $Q = 0.72$, negligible ejecta). As evidenced in Fig. 5, each dynamical ejecta model provides a different result. With KF's model, the most compact EOSs are allowed, and the lesser are ruled out; DU's model disallows all EOSs; and we see that no claims can be made about the EOS when using NAL's model. That the different models are able to produce such discrepant results for unequal mass systems suggests that further simulations in this regime are needed in order to properly calibrate future ejecta models to a broader region of parameter space. We should also note that this study is highly idealized, neglecting uncertainties due to the ejecta composition and geometry, nuclear reactions, and photon transport in the outflows. Our only objective is to assess (dis)agreement between existing outflow models, and we see that even if differences between models were the sole source of uncertainty, that uncertainty would already be extremely limiting. An additional potential source of uncertainty that was not explored in this paper is that which arises from the

choice of NR simulations. In other words, we expect that whichever set of simulations serves as training data will have an impact on the fitting formulas. For example, as noted in Nedora *et al.* [24], the treatment of microphysics in NR simulations currently has a significant impact on model performance and results. However, with increasingly detailed simulations that cover a larger set of parameters, we hope that in the future these models can be used to place robust constraints on the amount of ejecta from BNS mergers.

ACKNOWLEDGMENTS

A. H. and F. F. gratefully acknowledge support from the DOE through Grant No. DE-SC0020435, and from NASA through Grant No. 80NSSC18K0565. G. R. and S. M. N. are grateful for financial support from the Nederlandse Organisatie voor Wetenschappelijk Onderzoek (NWO) through the Projectruimte and VIDI Grants (Nissanke). S. M. N. also acknowledges financial support from the NWO sector plan.

[1] B. P. Abbott, R. Abbott, T. D. Abbott, F. Acernese, K. Ackley, C. Adams, T. Adams, P. Addesso, R. X. Adhikari, V. B. Adya *et al.*, Multi-messenger observations of a binary neutron star merger, Astrophys. J. **848**, L12 (2017).

[2] B. P. Abbott *et al.* (LIGO Scientific and Virgo Collaborations), Tests of General Relativity with GW170817, Phys. Rev. Lett. **123**, 011102 (2019).

[3] J. M. Lattimer and D. N. Schramm, The tidal disruption of neutron stars by black holes in close binaries, Astrophys. J. **210**, 549 (1976).

[4] C. Freiburghaus, S. Rosswog, and F.-K. Thielemann, R-process in neutron star mergers, Astrophys. J. **525**, L121 (1999).

[5] D. Kasen, B. Metzger, J. Barnes, E. Quataert, and E. Ramirez-Ruiz, Origin of the heavy elements in binary neutron-star mergers from a gravitational-wave event, Nature (London) **551**, 80 (2017).

[6] L.-X. Li and B. Paczynski, Transient events from neutron star mergers, Astrophys. J. **507**, L59 (1998).

[7] É. É. Flanagan and T. Hinderer, Constraining neutron-star tidal Love numbers with gravitational-wave detectors, Phys. Rev. D **77**, 021502 (2008).

[8] B. Abbott, R. Abbott, T. Abbott, F. Acernese, K. Ackley, C. Adams, T. Adams, P. Addesso, R. Adhikari, V. Adya *et al.*, Gw170817: Measurements of Neutron Star Radii and Equation of State, Phys. Rev. Lett. **121**, 161101 (2018).

[9] J. Barnes and D. Kasen, Effect of a high opacity on the light curves of radioactively powered transients from compact object mergers, Astrophys. J. **775**, 18 (2013).

[10] R. T. Wollaeger, C. L. Fryer, E. A. Chase, C. J. Fontes, M. Ristic, A. L. Hungerford, O. Korobkin, R. O'Shaughnessy, and A. M. Herring, A broad grid of 2d kilonova emission models, Astrophys. J. **918**, 10 (2021).

[11] M. W. Coughlin, T. Dietrich, Z. Doctor, D. Kasen, S. Coughlin, A. Jerkstrand, G. Leloudas, O. McBrien, B. D. Metzger, R. O'Shaughnessy, and S. J. Smartt, Constraints on the neutron star equation of state from AT2017gfo using radiative transfer simulations, Mon. Not. R. Astron. Soc. **480**, 3871 (2018).

[12] M. Bulla, Possis: Predicting spectra, light curves, and polarization for multidimensional models of supernovae and kilonovae, Mon. Not. R. Astron. Soc. **489**, 5037 (2019).

[13] S. Wanajo, Y. Sekiguchi, N. Nishimura, K. Kiuchi, K. Kyutoku, and M. Shibata, Production of all the *r*-process nuclides in the dynamical ejecta of neutron star mergers, Astrophys. J. Lett. **789**, L39 (2014).

[14] D. Radice, F. Galeazzi, J. Lippuner, L. F. Roberts, C. D. Ott, and L. Rezzolla, Dynamical mass ejection from binary neutron star mergers, Mon. Not. R. Astron. Soc. **460**, 3255 (2016).

[15] D. M. Siegel and B. D. Metzger, Three-Dimensional General-Relativistic Magnetohydrodynamic Simulations of Remnant Accretion Disks from Neutron Star Mergers: Outflows and *r*-Process Nucleosynthesis, Phys. Rev. Lett. **119**, 231102 (2017).

[16] R. Fernández, A. Tchekhovskoy, E. Quataert, F. Foucart, and D. Kasen, Long-term GRMHD simulations of neutron star merger accretion discs: Implications for electromagnetic counterparts, Mon. Not. R. Astron. Soc. **482**, 3373 (2019).

[17] L. Dessart, C. D. Ott, A. Burrows, S. Rosswog, and E. Livne, Neutrino signatures and the neutrino-driven wind in binary neutron star mergers, Astrophys. J. **690**, 1681 (2009).

[18] O. Just, A. Bauswein, R. Ardevol Pulpillo, S. Goriely, and H.-T. Janka, Comprehensive nucleosynthesis analysis for ejecta of compact binary mergers, Mon. Not. R. Astron. Soc. **448**, 541 (2015).

[19] R. Fernández and B. D. Metzger, Delayed outflows from black hole accretion tori following neutron star binary coalescence, Mon. Not. R. Astron. Soc. **435**, 502 (2013).

[20] T. Yamamoto, M. Shibata, and K. Taniguchi, Simulating coalescing compact binaries by a new code (SACRA), Phys. Rev. D **78**, 064054 (2008).

[21] T. Dietrich and M. Ujevic, Modeling dynamical ejecta from binary neutron star mergers and implications for electromagnetic counterparts, Classical Quantum Gravity **34**, 105014 (2017).

[22] D. Radice, A. Perego, K. Hotokezaka, S. A. Fromm, S. Bernuzzi, and L. F. Roberts, Binary neutron star mergers: Mass ejection, electromagnetic counterparts, and nucleosynthesis, Astrophys. J. **869**, 130 (2018).

[23] C. J. Krüger and F. Foucart, Estimates for disk and ejecta masses produced in compact binary mergers, Phys. Rev. D **101**, 103002 (2020).

[24] V. Nedora, F. Schianchi, S. Bernuzzi, D. Radice, B. Daszuta, A. Endrizzi, A. Perego, A. Prakash, and F. Zappa, Mapping

dynamical ejecta and disk masses from numerical relativity simulations of neutron star mergers, Classical Quantum Gravity **39**, 015008 (2022).

[25] K. Hotokezaka, K. Kiuchi, K. Kyutoku, H. Okawa, Y.-I. Sekiguchi, M. Shibata, and K. Taniguchi, Mass ejection from the merger of binary neutron stars, Phys. Rev. D **87**, 024001 (2013).

[26] A. Bauswein, S. Goriely, and H.-T. Janka, Systematics of dynamical mass ejection, nucleosynthesis, and radioactively powered electromagnetic signals from neutron-star mergers, Astrophys. J. **773**, 78 (2013).

[27] T. Dietrich, S. Bernuzzi, M. Ujevic, and B. Brügmann, Numerical relativity simulations of neutron star merger remnants using conservative mesh refinement, Phys. Rev. D **91**, 124041 (2015).

[28] L. Lehner, S. L. Liebling, C. Palenzuela, O. L. Caballero, E. O'Connor, M. Anderson, and D. Neilsen, Unequal mass binary neutron star mergers and multimessenger signals, Classical Quantum Gravity **33**, 184002 (2016).

[29] Y. Sekiguchi, K. Kiuchi, K. Kyutoku, M. Shibata, and K. Taniguchi, Dynamical mass ejection from the merger of asymmetric binary neutron stars: Radiation-hydrodynamics study in general relativity, Phys. Rev. D **93**, 124046 (2016).

[30] T. Dietrich, M. Ujevic, W. Tichy, S. Bernuzzi, and B. Brügmann, Gravitational waves and mass ejecta from binary neutron star mergers: Effect of the mass ratio, Phys. Rev. D **95**, 024029 (2017).

[31] J. M. Lattimer and M. Prakash, Neutron star structure and the equation of state, Astrophys. J. **550**, 426 (2001).

[32] K. Kiuchi, K. Kyutoku, M. Shibata, and K. Taniguchi, Revisiting the lower bound on tidal deformability derived by at 2017gfo, Astrophys. J. **876**, L31 (2019).

[33] Y. Sekiguchi, K. Kiuchi, K. Kyutoku, and M. Shibata, Dynamical mass ejection from binary neutron star mergers: Radiation-hydrodynamics study in general relativity, Phys. Rev. D **91**, 064059 (2015).

[34] T. Vincent, F. Foucart, M. D. Duez, R. Haas, L. E. Kidder, H. P. Pfeiffer, and M. A. Scheel, Unequal mass binary neutron star simulations with neutrino transport: Ejecta and neutrino emission, Phys. Rev. D **101**, 044053 (2020).

[35] A. Perego, S. Bernuzzi, and D. Radice, Thermodynamics conditions of matter in neutron star mergers, Eur. Phys. J. A **55**, 124 (2019).

[36] S. Bernuzzi, M. Breschi, B. Daszuta, A. Endrizzi, D. Logoteta, V. Nedora, A. Perego, D. Radice, F. Schianchi, F. Zappa, I. Bombaci, and N. Ortiz, Accretion-induced prompt black hole formation in asymmetric neutron star mergers, dynamical ejecta, and kilonova signals, Mon. Not. R. Astron. Soc. **497**, 1488 (2020).

[37] V. Nedora, S. Bernuzzi, D. Radice, A. Perego, A. Endrizzi, and N. Ortiz, Spiral-wave wind for the blue kilonova, Astrophys. J. **886**, L30 (2019).

[38] T. Dietrich, M. W. Coughlin, P. T. H. Pang, M. Bulla, J. Heinzel, L. Issa, I. Tews, and S. Antier, Multimessenger constraints on the neutron-star equation of state and the hubble constant, Science **370**, 1450 (2020).

[39] K. Hotokezaka, K. Kyutoku, H. Okawa, M. Shibata, and K. Kiuchi, Binary neutron star mergers: Dependence on the nuclear equation of state, Phys. Rev. D **83**, 124008 (2011).

[40] T. Damour and A. Nagar, Relativistic tidal properties of neutron stars, Phys. Rev. D **80**, 084035 (2009).

[41] K. Yagi and N. Yunes, Approximate universal relations for neutron stars and quark stars, Phys. Rep. **681**, 1 (2017).

[42] M. W. Coughlin, T. Dietrich, B. Margalit, and B. D. Metzger, Multimessenger bayesian parameter inference of a binary neutron star merger, Mon. Not. R. Astron. Soc. **489**, L91 (2019).

[43] M. Agathos, F. Zappa, S. Bernuzzi, A. Perego, M. Breschi, and D. Radice, Inferring prompt black-hole formation in neutron star mergers from gravitational-wave data, Phys. Rev. D **101**, 044006 (2020).

[44] B. P. Abbott, R. Abbott, T. D. Abbott, S. Abraham, F. Acernese, K. Ackley, C. Adams, R. X. Adhikari, V. B. Adya, C. Affeldt *et al.*, Gw190425: Observation of a compact binary coalescence with total mass $\sim 3.4\ m_{\odot}$, Astrophys. J. **892**, L3 (2020).

[45] V. Doroshenko, V. Suleimanov, G. Pühlhofer, and A. Santangelo, A strangely light neutron star within a supernova remnant, Nat. Astron. **6**, 1 (2022).

[46] A. Camilletti, L. Chiesa, G. Ricigliano, A. Perego, L. C. Lippold, S. Padamata, S. Bernuzzi, D. Radice, D. Logoteta, and F. M. Guercilena, Numerical relativity simulations of the neutron star merger GW190425: Microphysics and mass ratio effects, Mon. Not. R. Astron. Soc. **516**, 4760 (2022).

[47] H.-Y. Chen, S. Vitale, and F. Foucart, The relative contribution to heavy metals production from binary neutron star mergers and neutron star–Black hole mergers, Astrophys. J. Lett. **920**, L3 (2021).

[48] L. Lindblom, Spectral representations of neutron-star equations of state, Phys. Rev. D **82**, 103011 (2010).

[49] G. Raaijmakers, S. Nissanke, F. Foucart, M. M. Kasliwal, M. Bulla, R. Fernandez, A. Henkel, T. Hinderer, K. Hotokezaka, K. Lukošiūtė, T. Venumadhav, S. Antier, M. W. Coughlin, T. Dietrich, and T. D. P. Edwards, The challenges ahead for multimessenger analyses of gravitational waves and kilonova: A case study on GW190425, Astrophys. J. **922**, 269 (2021).